Wei-Liang Chen
Graduate Student
Department of Mechanical Engineering,
National Chiao Tung University,
Hsinchu 30010,
Taiwan, R.O.C.

Chung-Biau Tsay[1]
Chair Professor
Department of Mechanical and
Computer-Aided Engineering,
Feng Chia University,
Taichung 40724,
Taiwan, R.O.C.
e-mail: cbtsay@mail.nctu.edu.tw

Contact Characteristics of Recess Action Worm Gear Drives With Double-Depth Teeth

Based on the previously developed mathematical model of a series of recess action (RA) worm gear drive (i.e., semi RA, full RA, and standard proportional tooth types) with double-depth teeth, the tooth contact analysis (TCA) technique is utilized to investigate the kinematic error (KE), contact ratio (CR), average contact ratio (ACR), instantaneous contact teeth (ICT) under different assembly conditions. Besides, the bearing contact and contact ellipse are studied by applying the surface topology method. Three numerical examples are presented to demonstrate the influence of the assembly errors and design parameters of the RA worm gear drive on the KE, CR, ACR, ICT, and contact patterns. [DOI: 10.1115/1.4004985]

Keywords: recess action, RA worm gear drive, double-depth teeth, kinematic error, average contact ratio, instantaneous contact teeth, tooth contact analysis

1 Introduction

Few of gears, such as indexing gears, are applied to transmit precise control of angular motion. Some of indexing gears usually operate in the open air, or only use grease lubrication, especially that are used to drive military weapons, radio telescopes, satellite tracking antennas, etc. They need to operate under conditions of lower friction, more smooth and stable than equivalent gears. It is well-known that recess action gears (abbreviated to RA gears) have less wear with lower friction and less noise. Buckingham [1] interpreted that friction of recess action is lower than that of approach action when gears are in meshing. Buckingham [2] also indicated that one of worm gear drives, the deep-tooth cylindrical worm drive, was manufactured by Delava-Holroyd, Inc., and employed to precise rotation of the heavy 200-in. Mt. Palomar telescope. It has also been applied to a large range of finders. This worm gear drive is similar to that of the conventional type, but it is actually modified into a full RA worm gear drive with double-depth teeth and low pressure angle. Compared with the conventional type of worm gear drives, these modifications result in a large number of teeth in contact and high recess action inducing lower friction. Benefits of multiple tooth contact not only reduces kinematic errors but also averages the sum of all tooth errors. Crosher [3] interpreted that Zahnradfabrik OTT in Germany has developed worm gear sets having a small backlash, and OTT's specifications were also satisfied the minimum total composite error in precise positioning. They were designed with a very high contact ratio in order to have a uniform and constant contact. This can be achieved by designing a worm gear drive with a lower pressure angle, very long tooth flanks and a larger number of worm gear teeth, etc. However, the limitation is the narrowness at the top of the teeth and the worm helix. Therefore, contact characteristic investigations on worm gear drives, semi RA, full RA, and standard proportional tooth types, with double-depth teeth is needed and proposed herein.

The bearing contact, kinematic error (KE), and contact ellipse can be simulated by the tooth contact analysis (TCA) [4,5]. Litvin and Kin [6] also proposed a generalized TCA algorithm to determine the position of transfer points where an ideal contact line will turn into a real contact point. The influences of rotation axial misalignments and center distance offset on the conjugate worm gear set were also investigated in their study. Tsay [7] applied TCA techniques to simulate the meshing conditions for involute helical gears and proposed the compensation method to reduce the KEs induced by horizontal axial misalignments. Lin et al. [8] performed TCA for hypoid gears. Fang and Tsay [9–11] derived mathematical models of the ZK, ZN, and ZE-type worm gear drives generated by oversize hob cutters, based on their hobbing mechanisms, respectively. Besides, further investigations on bearing contacts and KEs of these types of worm gear drives were also studied. They also investigated the bearing contacts and KEs of a noncoupled combination of ZE-type and ZK-type worm gear set [12]. Shigley and Mischke [13] defined the contact ratio (CR) of a gear pair as the average number of teeth in contact during the gear meshing. The CR can be also defined by the gear rotation angle, measured from the starting point to the end point of contact, divided by the angle formed by two successive teeth. Bair and Tsay [14,15] studied the bearing contact, KE, CR, and average contact ratio (ACR) of the ZK-type dual-lead worm gear drive. Janninck [16] proposed a method for designing an oversize hob cutter to cut worm gears. The contact surface separation method was also adopted to show the results of his study. Litvin et al. [17] developed a method to localize bearing contacts for various gear pairs and proposed a method to absorb the discontinuous linear KEs caused by gear axial misalignments. Chen and Tsay [18] developed the mathematical model of the ZK-type worm and ZN-type worm gear drive meshing under a non-ninety-degree crossing angle, and CR, instantaneous contact teeth (ICT) and ACR were also investigated. Colbourne [19] investigated the undercutting, interference and nonconjugate contact of the ZK-type worm gear drives. Simon [20] proposed a new type of worm gear drive, whose worm profile is concave, that the TCA, the load distribution calculation, and the thermal elastohydrodynamic lubrication analysis of different types of worm gears have been carried out, and the obtained results show the advantages. Litvin et al. [21] simulated the TCA of Klingelnberg-type worm gear drives, whose worm is generating by an oversize hob cutter and mismatch geometries of hob and worm of the drive. Seol and Litvin [22] modified involute geometry of Klingelnberg and Flender type worm gear drives to provide a localized and stable bearing contact with reduced the misalignment sensitivity. Seol [23] obtained the localization of bearing contact at the longitudinal direction, based on proper mismatch of the surfaces of the hob and the worm. The developed approach is applicable for all types of single-enveloping worm gear drive.

[1]Corresponding author.
Contributed by the Power Transmission and Gearing Committee of ASME for publication in the Journal Of Mechanical Design. Manuscript received January 17, 2011; final manuscript received August 10, 2011; published online November 11, 2011. Assoc. Editor: Prof. Philippe Velex.

Up to now, only few researches have been investigated on the RA worm gears. Buckingham [1] proposed how to design RA worm gears. Yang [24] proposed an interactive computer graphics program to apply to an optimum RA worm gear design. Siegal and Mabie [25] developed a method to maximize the ratio of recess action to approach action by determining the individual hob offsets for a pair of spur gears designed to operate under nonstandard center distances. Meng and Chen [26] investigated theoretically and experimentally the scuffing resistance of full RA worm gears, in comparison with semi RA and standard ones. It appeared that full RA worm gears might prefer the pitting resistance and plastic-flow state to scuffing resistance in some extent than those of the others.

However, computer simulation, TCA, stress analysis, etc., of RA worm gears have not been studied yet. The aim of this paper is to investigate the KE, CR, ACR, and ICT of the full RA worm gear drive with double-depth teeth by applying the TCA technique under different assembly conditions. Besides, the bearing contact and contact ellipse are also studied by using the surface topology method.

2 Approach Action and Recess Action of Meshings for the Semi RA, Full RA, and Standard Proportional Tooth Worm Gear Drives

Figure 1 shows three types of worm gear drive meshing, semi RA, full RA, and standard proportional tooth worm gear drives, with double-depth teeth at the same standard center distance. Figure 1(*a*) shows the worm gear drive with standard proportional

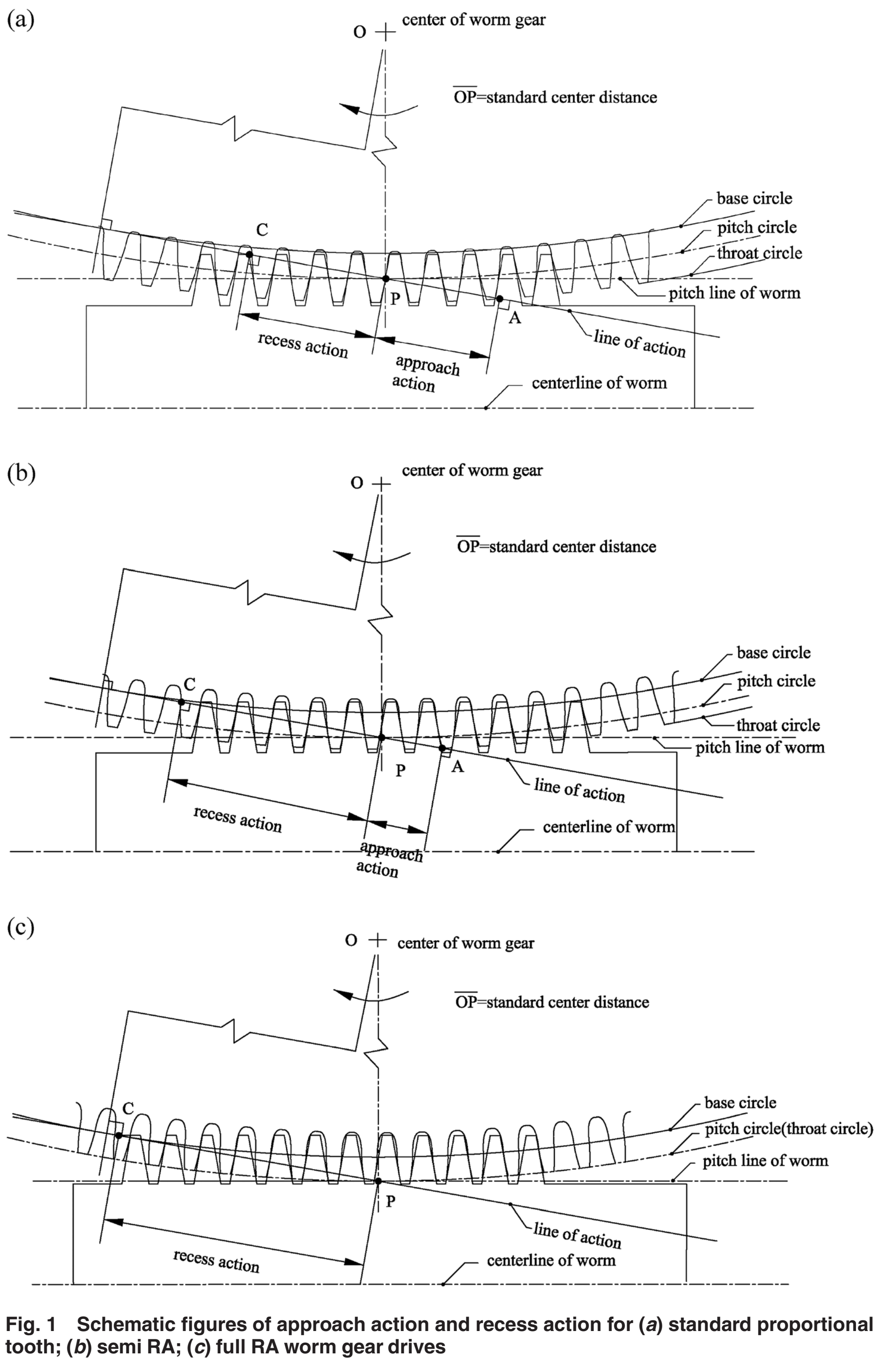

Fig. 1 Schematic figures of approach action and recess action for (*a*) standard proportional tooth; (*b*) semi RA; (*c*) full RA worm gear drives

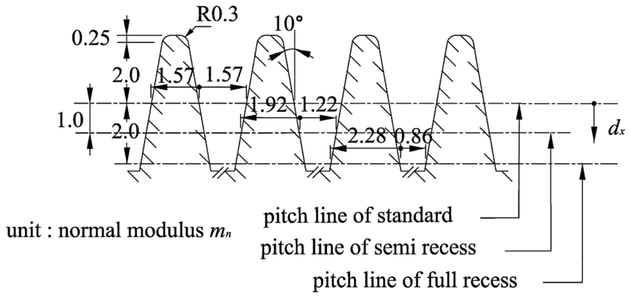

Fig. 2 Normal section of hob cutter with double-depth teeth, low pressure angle and varying pitch lines

tooth meshing system. As contact progresses from point A (starting point of tooth engagement) to point P (pitch point), there is an approach action, while recess action occurs from point P to point C (final point of tooth engagement). It is noted that two parts of line of action for approach action and recess action are of equal contributions for the standard proportional tooth meshing system.

The RA gear can eliminate the amount of friction by reducing the approach action, or increasing the recess action. Figure 1(*c*) is the full RA worm gear meshing system obtained by having the pitch line of the worm tangent to the throat circle of the worm gear. In this case, the pitch circle and throat circle of the full RA worm gear are identical. The worm is made larger and the worm gear is smaller, so that the lead of worm is equal to the circular pitch of the worm gear at pitch circle or throat circle. This results in the existence of only the recess action in the process of worm gear drive mating. As shown in Figs. 1(*b*) and 1(*c*), both semi RA and full RA worm gear drives have a change in the contact conditions between engaging teeth.

3 RA Worm Gears With Double-Depth Teeth Generated by Different Recess of Hob Cutters

RA worm gears can be manufactured with a hob cutter and hobbing machine, but consideration on varying pitch line of hob cutter with respect to the generated RA worm gear is needed. In this study, let us design the hob cutter different from that of the conventional one. Figure 2 shows the normal section of hob cutter that its tooth form is a straight-lined edge shape based on the ZN worm-type of ISO classification. To design RA worm gear drives with double-depth teeth, the pressure angle of hob cutter is reduced from the normally used 20 deg and 22.5 deg to a minimum of 10 deg [2]. This should pay more attention on the checking of the teeth of hob cutter and the generated RA worm gear should not appear pointed teeth. The pitch lines of the hob cutter in generating semi RA and full RA worm gears become $d_x = 1.0$ and 2.0 of normal modulus, m_n, below the middle of cutting tooth height, respectively, as shown in Fig. 2. Where d_x is the distance measured from the middle of cutting blade height to the varying pitch line (also refer to Figs. 3(*b*) and 3(*d*)). Thus, tooth thicknesses of the generated semi RA and full RA worm gears at their normal pitch circles become 1.22 and 0.86w_n, and their normal throat radii are $(T_2+2)m_n/2$ mm and $T_2 m_n/2$ mm, individually. Symbol T_2 denotes the tooth number of the generated RA worm gear. The above design gives different proportional changes of addendum and dedendum of hob cutter in generating semi RA and full RA worm gears. Especially, for a full RA worm gear, the pitch circle and throat circle are identical. Besides, the standard proportional tooth worm gear is a special case of the RA type worm gear when d_x equals 0, no doubt, the pitch line of the hob cutter is at the middle of cutting tooth height. This gives that tooth thickness of the generated worm gear at its normal pitch circle is $1.51m_n$, and normal throat radius is $(T_2+4)m_n/2$ mm.

4 Tooth Surface Equation of the ZN Worm-Type Hob Cutter

Theoretically, the ZN worm is cut by a straight-lined edge cutting blade, and the worm gear is produced by a worm-type hob cutter, which is identical to the worm. The bearing contact of the worm gear drive is in line contact. This may result in an edge contact under gear assembly errors. In order to obtain the worm gear drive with point contacts, the worm gear usually is generated by an oversize worm-type hob cutter. The oversize ZN-type hob cutter surface can be generated by a blade with the straight-lined edge, performing a screw motion with respect to the rotational

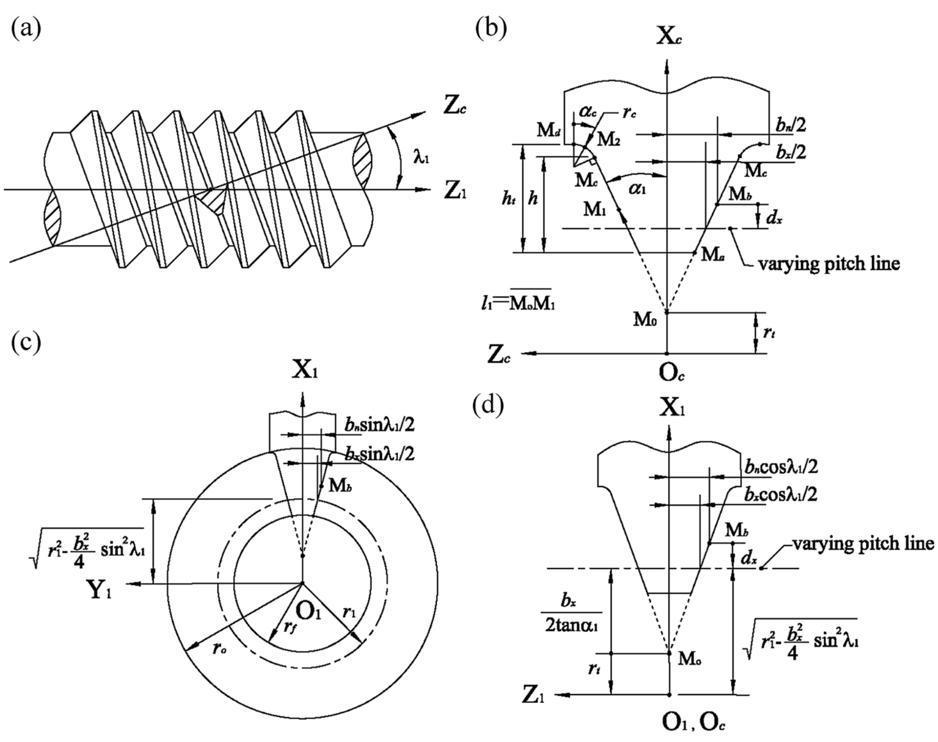

Fig. 3 ZN worm-type hob cutter with varying pitch lines represented by parameter d_x

axis of hob cutter. The cutting blade is installed on the groove normal section of the hob cutter, as shown in Fig. 3(*a*). λ_1 designates the lead angle of hob cutter, while a_1 symbolizes the half-apex blade angle formed by the straight-lined edge blade and X_c-axis, as illustrated in Fig. 3(*b*). Symbols r_o, r_f, h, and d_x are design parameters of the hob cutter, as shown in Figs. 3(*b*)–3(*d*). l_1 denotes a design parameter of the cutting blade surface starting from the intersection point M_0 of the two straight-lined edges to the end point M_c. And the moving point M_1 represents any point of the cutting blade surface moving from the initial point M_a to the end point M_c. It is noted that point M_b is the middle point of $\overline{M_aM_c}$. Figure 4 shows the relationship among the coordinate systems $S_c(X_c, Y_c, Z_c)$, $S_1(X_1, Y_1, Z_1)$, and $S_f(X_f, Y_f, Z_f)$, where S_c is the blade coordinate system, coordinate system S_1 is rigidly connected to the hob cutter tooth surface, and S_f is the reference coordinate system. The inclined angle λ_1, formed by axes Z_c and Z_f, is the lead angle of hob cutter. The tooth surface equation of the ZN worm-type hob cutter can be obtained by considering the blade coordinate system, S_c performs a screw motion with respect to the fixed coordinate system S_f. Therefore, the surface equation of ZN worm-type hob cutter $\mathbf{R}_1$ is represented in coordinate system S_1 as follows:

$$\mathbf{R}_1 = \begin{bmatrix} (r_t + l_1\cos\alpha_1)\cos\theta_1 \mp l_1\sin\lambda_1\sin\alpha_1\sin\theta_1 \\ -(r_t + l_1\cos\alpha_1)\sin\theta_1 \mp l_1\sin\lambda_1\sin\alpha_1\cos\theta_1 \\ \pm\, l_1\cos\lambda_1\sin\alpha_1 - p_1\theta_1 \\ 1 \end{bmatrix} \tag{1}$$

where θ_1 is the surface parameter of hob cutter rotation angle. p_1 denotes the lead-per-radian revolution of the hob cutter's surface. In Eq. (1), the upper sign represents the right-side hob cutter surface, while the lower sign indicates the left-side hob cutter surface, and r_t can be expressed as follows:

$$r_t = \sqrt{r_1^2 - \left(\frac{b_x}{2}\sin\lambda_1\right)^2} - \frac{b_x}{2\tan\alpha_1} \tag{2}$$

$$b_x = b_n - 2d_x\tan\alpha_1 \tag{3}$$

where r_1 denotes pitch radius of the oversize ZN worm-type hob cutter, and $b_n = \pi m_n/2$.

5 Normal Vectors and Equation of Meshing of the ZN Worm-Type Hob Cutter and RA Worm Gear

The normal vector $\mathbf{N}_1$ and unit normal vector $\mathbf{n}_1$ of the straight-lined edge hob cutter surface, represented in coordinate system S_1 can be obtained by

$$\mathbf{N}_1 = \frac{\partial\mathbf{R}_1}{\partial l_1}\times\frac{\partial\mathbf{R}_1}{\partial\theta_1} = \begin{bmatrix} N_{x1} \\ N_{y1} \\ N_{z1}\end{bmatrix} \quad\text{and}\quad \mathbf{n}_1 = \frac{\mathbf{N}_1}{|\mathbf{N}_1|} = \begin{bmatrix} n_{x1} \\ n_{y1} \\ n_{z1}\end{bmatrix} \tag{4}$$

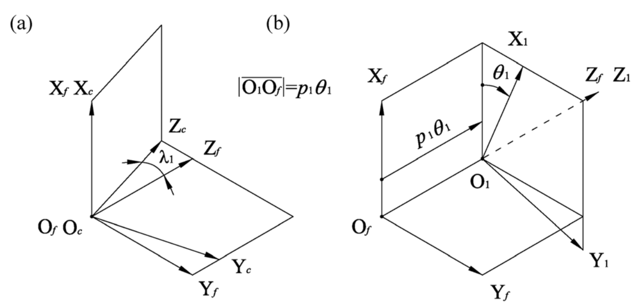

Fig. 4 Coordinate systems for (*a*) hob cutter setting with an inclined lead angle; (*b*) screw surface generation of ZN worm-type hob cutter

where

$$\frac{\partial\mathbf{R}_1}{\partial l_1} = \begin{bmatrix} \cos\alpha_1\cos\theta_1 \mp \sin\alpha_1\sin\lambda_1\sin\theta_1 \\ -\cos\alpha_1\sin\theta_1 \mp \sin\alpha_1\sin\lambda_1\cos\theta_1 \\ \pm\sin\alpha_1\cos\lambda_1 \end{bmatrix} \tag{5}$$

and

$$\frac{\partial\mathbf{R}_1}{\partial\theta_1} = \begin{bmatrix} -(r_t + l_1\cos\alpha_1)\sin\theta_1 \mp l_1\sin\lambda_1\sin\alpha_1\cos\theta_1 \\ -(r_t + l_1\cos\alpha_1)\cos\theta_1 \pm l_1\sin\lambda_1\sin\alpha_1\sin\theta_1 \\ -p_1 \end{bmatrix} \tag{6}$$

6 Tooth Surface Equation of the RA Worm Gear With Double-Depth Teeth

According to the worm gear generation mechanism, as shown in Fig. 5, the locus equation of the hob cutter $\mathbf{R}_2$, expressed in coordinate system S_2, is obtained as follows:

$$\mathbf{R}_2 = \begin{bmatrix} a_{11}X_1 + a_{12}Y_1 + \sin\gamma_1\sin\phi_2 Z_1 - \cos\phi_2 C_1 \\ a_{21}X_1 + a_{22}Y_1 + \sin\gamma_1\cos\phi_2 Z_1 - \sin\phi_2 C_1 \\ -\sin\gamma_1\sin\phi_1 X_1 - \sin\gamma_1\cos\phi_1 Y_1 + \cos\gamma_1 Z_1 \\ 1 \end{bmatrix} \tag{7}$$

where

$$\begin{aligned} a_{11} &= \cos\phi_1\cos\phi_2 + \cos\gamma_1\sin\phi_1\sin\phi_2, \\ a_{12} &= -\sin\phi_1\cos\phi_2 + \cos\gamma_1\cos\phi_1\sin\phi_2, \\ a_{21} &= -\cos\phi_1\sin\phi_2 + \cos\gamma_1\sin\phi_1\cos\phi_2, \\ a_{22} &= \sin\phi_1\sin\phi_2 + \cos\gamma_1\cos\phi_1\cos\phi_2, \end{aligned} \tag{8}$$

and

where $\phi_2 = \frac{T_1}{T_2}\phi_1$, and T_1, T_2, ϕ_1, and ϕ_2 are tooth numbers and rotational angles of the hob cutter and generated RA worm gear, respectively. C_1 is the cutting center distance, and γ_1 is the cutting crossing angle. X_1, Y_1, and Z_1 are three position components of ZN worm-type hob cutter $\mathbf{R}_1$.

It is noted that the worm gear is cut by a worm-type hob cutter, which is identical to the worm. Similarly, the unit normal vector of RA worm gear $\mathbf{n}_2$, expressed in coordinate system S_2, is obtained as follows:

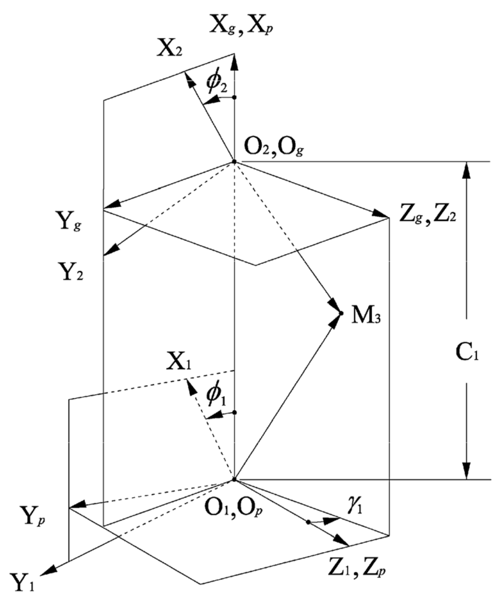

Fig. 5 Coordinate systems between ZN worm-type hob cutter and RA worm gear

$$\mathbf{n}_2 = \begin{bmatrix} n_{x2} \\ n_{y2} \\ n_{z2} \end{bmatrix} = \begin{bmatrix} a_{11}n_{x1} + a_{12}n_{y1} + \sin\gamma_1 \sin\phi_2 n_{z1} \\ a_{21}n_{x1} + a_{22}n_{y1} + \sin\gamma_1 \cos\phi_2 n_{z1} \\ -\sin\gamma_1 \sin\phi_1 n_{x1} - \sin\gamma_1 \cos\phi_1 n_{y1} + \cos\gamma_1 n_{z1} \end{bmatrix} \quad (9)$$

where n_{x1}, n_{y1}, and n_{z1} are components of the unit normal vector of the oversize ZN worm-type hob cutter.

The tooth surface equation of the oversize ZN worm-type hob cutter circular tip in generating RA worm gear is neglected, because it is not involved in the TCA simulation proposed in this paper. Hence, those parameters, α_c, γ_c, and h, with respect to the circular tip of ZN worm-type hob cutter are not concerned.

7 Equation of Meshing Between the Hob Cutter and Generated RA Worm Gears

In the worm gear generation process, the hob cutter and generated RA worm gear tooth surfaces are never embedded into each other, i.e., the relative velocity of the generated RA worm gear with respect to the hob cutter is perpendicular to their common normal vector $\mathbf{N}_1$ at any cutting instant. Therefore, the equation of meshing of the hob cutter and generated RA worm gear can be expressed as follows [4]:

$$\mathbf{N}_1 \bullet \mathbf{V}_{12}^{(1)} = \mathbf{N}_1 \bullet (\mathbf{V}_1^{(1)} - \mathbf{V}_2^{(1)}) = 0 \quad (10)$$

where $\mathbf{V}_1^{(1)}$ and $\mathbf{V}_2^{(1)}$ denote the velocities of the hob cutter and generated RA worm gear, respectively, and superscript "(1)" indicates the velocities are represented in coordinate system S_1. Equation (10) is the equation of meshing of the hob cutter and generated RA worm gear.

According to Fig. 5, the relative velocity of the generated RA worm gear with respect to the hob cutter represented in coordinate system S_1 can be obtained by

$$\mathbf{V}_{12}^{(1)} = (\boldsymbol{\omega}_1^{(1)} - \boldsymbol{\omega}_2^{(1)}) \times \mathbf{R}_1 - \overline{\mathbf{O_1O_2}}^{(1)} \times \omega_2^{(1)} \quad (11)$$

where $\boldsymbol{\omega}_1^{(1)}$ and $\boldsymbol{\omega}_2^{(1)}$ are the angular velocities of the hob cutter and the generated RA worm gear, respectively, and they can be expressed in coordinate systems S_1 as follows:

$$\boldsymbol{\omega}_1^{(1)} = \omega_1 [0 \quad 0 \quad 1]^{\mathrm{T}} \quad (12)$$

and

$$\boldsymbol{\omega}_1^{(1)} = \omega_1 \begin{bmatrix} -m_{21}\sin\gamma_1 \sin\phi_1 \\ -m_{21}\sin\gamma_1 \cos\phi_1 \\ m_{21}\cos\gamma_1 \end{bmatrix} \quad (13)$$

where $m_{21} = \phi_2/\phi_1$ is the angular velocity ratio of the generated RA worm gear to the hob cutter.

Similarly, according to Fig. 5, vector $\overline{\mathbf{O_1O_2}}$ can be obtained and expressed in coordinate system S_1 by

$$\overline{\mathbf{O_1O_2}}^{(1)} = \begin{bmatrix} \cos\phi_1 C_1 \\ -\sin\phi_1 C_1 \\ 0 \end{bmatrix} \quad (14)$$

Substituting Eqs. (1) and (12)–(14) into Eq. (11) yields

$$\mathbf{V}_{12}^{(1)} = \omega_1 \begin{bmatrix} (m_{21}\cos\gamma_1 - 1)\mathrm{Y}_1 + m_{21}(\sin\gamma_1\cos\phi_1\,\mathrm{Z}_1 + \cos\gamma_1\sin\phi_1\,\mathrm{C}_1) \\ -(m_{21}\cos\gamma_1 - 1)\mathrm{X}_1 + m_{21}(-\sin\gamma_1\sin\phi_1\,\mathrm{Z}_1 + \cos\gamma_1\cos\phi_1\,\mathrm{C}_1) \\ m_{21}\sin\gamma_1(-\cos\phi_1\mathrm{X}_1 + \sin\phi_1\mathrm{Y}_1 + \mathrm{C}_1) \end{bmatrix} \quad (15)$$

Substituting Eqs. (4) and (15) into Eq. (10), the equation of meshing of the hob cutter and generated RA worm gear can be expressed as follows:

$$\begin{aligned} f(l_1,\theta_1,\phi_1(\phi_2)) = \omega_1\{&[(m_{21}\cos\gamma_1 - 1)\mathrm{Y}_1 + m_{21}(\cos\phi_1\sin\gamma_1\mathrm{Z}_1 \\ &+ \sin\phi_1\cos\gamma_1\mathrm{C}_1)]\mathrm{N}_{x1} + [-(m_{21}\sin\gamma_1 - 1)\mathrm{X}_1 \\ &+ m_{21}(-\sin\phi_1\sin\gamma_1\mathrm{Z}_1 + \cos\phi_1\cos\gamma_1\mathrm{C}_1)]\mathrm{N}_{y1} \\ &+ [m_{21}\sin\gamma_1(-\cos\phi_1\mathrm{X}_1 \\ &+ \sin\phi_1\mathrm{Y}_1 + \mathrm{C}_1)]\mathrm{N}_{z1}\} = 0, \end{aligned} \quad (16)$$

Equation (16) keeps the hob cutter and generated RA worm gear in tangency at every instant during the RA worm gear cutting process. According to the theory of gearing, the tooth surface of the generated RA worm gear can be obtained by considering the locus equation of the hob cutter and the equation of meshing, i.e., Eqs. (7) and (16), simultaneously.

8 Tooth Contact Analysis

Gears are applied to transmit power or motion, thus the tooth contact analysis should be performed. In general, the gear drive assembly errors are mainly consisted of center distance assembly error and vertical as well as horizontal angular assembly errors. In this study, influences of the axial misalignments and center distance assembly error on the contact path, KE, CR, and ICT are investigated.

8.1 Meshing Model and Analysis on KE. Figure 6 shows the schematic diagram that the RA worm gear drives mesh under three main assembly errors. These assembly errors can be expressed by changing the settings and orientations of the reference coordinate system S_u with respect to the fixed coordinate system S_w and to coordinate systems S_2 and S_3, respectively. Coordinate systems S_3 and S_2 are attached to the worm and the worm gear, respectively. The origins, O_w and O_3, of the fixed coordinate system S_w and the

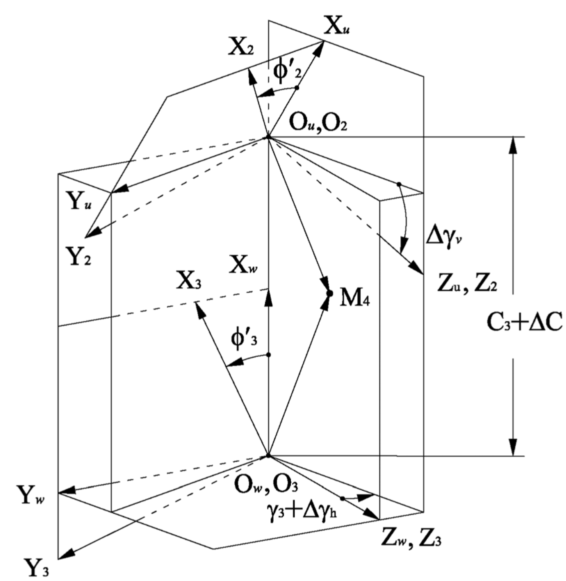

Fig. 6 Simulation of gear meshing with assembly errors

RA worm coordinate system S_3 are coincident. The reference coordinate system S_u relates two rotational coordinate systems, S_3 and S_2, of the RA worm and the RA worm gear with a center distance assembly error $C_3 + \Delta C$ and misaligned assembly crossing angles $\Delta\gamma_h$ and $\Delta\gamma_v$, respectively. C_3 and γ_3 are standard meshing center distance and crossing angle of the RA worm gear drive, respectively. It is noted that ΔC is the center distance assembly error, while $\Delta\gamma_h$ is the horizontal assembly crossing angle error, and $\Delta\gamma_v$ is the error of vertical assembly angle. The RA worm and worm gear rotate about their respective axes Z_3 and Z_2, through rotational angles ϕ'_3 and ϕ'_2, relative to their reference coordinate systems S_w and S_u, respectively.

In order to calculate the instantaneous contact point M_4 of the contact tooth surfaces, as shown in Fig. 6, the position vectors and unit normal vectors of the RA worm and RA worm gear should be represented in the same coordinate system, say coordinate system S_w. In the mating process, the position vectors of the RA worm and worm gear should be the same and unit normal vectors must be collinear to each other at the instantaneous tooth contact point, owing to the tangency of two contacting gear tooth surfaces. Therefore

$$\mathbf{R}_w^{(3)} = \mathbf{R}_w^{(2)} \tag{17}$$

$$\mathbf{n}_w^{(3)} \times \mathbf{n}_w^{(2)} = 0 \tag{18}$$

where $\mathbf{R}_w^{(3)}$ and $\mathbf{n}_w^{(3)}$, $\mathbf{R}_w^{(2)}$ and $\mathbf{n}_w^{(2)}$ indicate the position vectors and unit normal vectors of the RA worm and worm gear tooth surfaces at their common contact point, respectively, expressed in fixed coordinate system S_w. Position vectors $\mathbf{R}_w^{(3)}$ and $\mathbf{R}_w^{(2)}$ expressed in Eq. (17) can be obtained by applying the following homogeneous coordinate transformation matrix equations:

$$\mathbf{R}_w^{(3)} = \mathbf{M}_{w3}\mathbf{R}_3^{(3)} \tag{19}$$

$$\mathbf{R}_w^{(2)} = \mathbf{M}_{wu}\mathbf{M}_{u2}\mathbf{R}_2^{(2)} = \mathbf{M}_{w2}\mathbf{R}_2^{(2)} \tag{20}$$

where $\mathbf{R}_3^{(3)}$ denotes the position vector of RA worm expressed in coordinate system S_3, which is similar to the position vector $\mathbf{R}_1$ of the ZN worm-type hob cutter as expressed in Eq. (1). $\mathbf{R}_2^{(2)}$ is the position vector of RA worm gear tooth surfaces, expressed in fixed coordinate system S_2, as shown in Eq. (7). In Eqs. (19) and (20), transformation matrices $\mathbf{M}_{w3}$ and $\mathbf{M}_{w2}$ can be obtained as follows:

$$\mathbf{M}_{w3} = \begin{bmatrix} \cos\phi'_3 & -\sin\phi'_3 & 0 & 0 \\ \sin\phi'_3 & \cos\phi'_3 & 0 & 0 \\ 0 & 0 & 1 & 0 \\ 0 & 0 & 0 & 1 \end{bmatrix} \tag{21}$$

and

$$\mathbf{M}_{w2} = \begin{bmatrix} \cos\Delta\gamma_v\cos\phi'_3 & -\cos\Delta\gamma_v\sin\phi'_2 & \sin\Delta\gamma_v & C_3+\Delta C \\ b_{21} & b_{22} & -\sin(\gamma_3+\Delta\gamma_h)\cos\Delta\gamma_v & 0 \\ b_{31} & b_{32} & \cos(\gamma_3+\Delta\gamma_h)\cos\Delta\gamma_v & 0 \\ 0 & 0 & 0 & 1 \end{bmatrix} \tag{22}$$

where

$$\begin{aligned} b_{21} &= \sin(\gamma_3+\Delta\gamma_h)\sin\Delta\gamma_v\cos\phi'_2 + \cos(\gamma_3+\Delta\gamma_h)\sin\phi'_2, \\ b_{22} &= -\sin(\gamma_3+\Delta\gamma_h)\sin\Delta\gamma_v\sin\phi'_2 + \cos(\gamma_3+\Delta\gamma_h)\cos\phi'_2, \\ b_{31} &= -\cos(\gamma_3+\Delta\gamma_h)\sin\Delta\gamma_v\cos\phi'_2 + \sin(\gamma_3+\Delta\gamma_h)\sin\phi'_2, \\ b_{32} &= \cos(\gamma_3+\Delta\gamma_h)\sin\Delta\gamma_v\sin\phi'_2 + \sin(\gamma_3+\Delta\gamma_h)\cos\phi'_2. \end{aligned} \tag{23}$$

and $b_{32} = \cos(\gamma_3+\Delta\gamma_h)\sin\Delta\gamma_v\sin\phi'_2 + \sin(\gamma_3+\Delta\gamma_h)\cos\phi'_2$.

Substituting Eqs. (1) and (21) into Eq. (19) obtains

$$\mathbf{R}_w^{(3)} = \begin{bmatrix} \cos\phi'_3 X_3 - \sin\phi'_3 Y_3 \\ \sin\phi'_3 X_3 + \cos\phi'_3 Y_3 \\ Z_3 \\ 1 \end{bmatrix} \tag{24}$$

and substituting Eqs. (7) and (22) into Eq. (20) results in

$$\mathbf{R}_w^{(2)} = \begin{bmatrix} \cos\Delta\gamma_v\cos\phi'_2 X_2 - \cos\Delta\gamma_v\sin\phi'_2 Y_2 + \sin\Delta\gamma_v Z_2 + (C_3+\Delta C) \\ b_{21}X_2 + b_{22}Y_2 - \sin(\gamma_3+\Delta\gamma_h)\cos\Delta\gamma_v Z_2 \\ b_{31}X_2 + b_{32}Y_2 + \cos(\gamma_3+\Delta\gamma_h)\cos\Delta\gamma_v Z_2 \\ 1 \end{bmatrix} \tag{25}$$

Similarly, unit normal vectors $\mathbf{n}_w^{(3)}$ and $\mathbf{n}_w^{(2)}$ expressed in Eq. (18) can be obtained by applying the following homogeneous coordinate transformation matrix equations:

$$\mathbf{n}_w^{(3)} = \mathbf{L}_{w3}\mathbf{n}_3^{(3)} \tag{26}$$

and

$$\mathbf{n}_w^{(2)} = \mathbf{L}_{wu}\mathbf{L}_{u2}\mathbf{n}_2^{(2)} = \mathbf{L}_{w2}\mathbf{n}_2^{(2)} \tag{27}$$

where $\mathbf{n}_3^{(3)}$ denotes the unit normal vector of RA worm expressed in coordinate system S_3, which is identical to the unit normal vector $\mathbf{n}_1$ of oversize ZN worm-type hob cutter as expressed in Eq. (4). $\mathbf{n}_2^{(2)}$ is the unit normal vector of RA worm gear expressed in fixed coordinate system S_2, as shown in Eq. (9). Matrices $\mathbf{L}_{w3}$ and $\mathbf{L}_{w2}$ can be obtained by deleting the last column and last row of matrices $\mathbf{M}_{w3}$ and $\mathbf{M}_{w2}$, expressed in Eqs. (21) and (22), respectively.

Substituting Eq. (4) into Eq. (26), one receives $\mathbf{n}_w^{(3)}$, expressed in coordinate system S_w, as follows:

$$\mathbf{n}_w^{(3)} = \begin{bmatrix} \cos\phi'_3 n_{x3} - \sin\phi'_3 n_{y3} \\ \sin\phi'_3 n_{x3} + \cos\phi'_3 n_{y3} \\ n_{z3} \end{bmatrix} \tag{28}$$

where n_{x3}, n_{y3}, and n_{z3} are three components of the unit normal vector of RA worm, expressed in coordinate system S_3.

Similarly, substituting Eq. (9) into Eq. (27) obtains $\mathbf{n}_w^{(2)}$, expressed in coordinate system S_w, as follows:

$$\mathbf{n}_w^{(2)} = \begin{bmatrix} \cos\Delta\gamma_v\cos\phi'_3 n_{x2} - \cos\Delta\gamma_v\sin\phi'_3 n_{y2} + \sin\Delta\gamma_v n_{z2} \\ b_{21}n_{x2} + b_{22}n_{y2} - \sin(\gamma_3+\Delta\gamma_v)\cos\Delta\gamma_v n_{z2} \\ b_{31}n_{x2} + b_{32}n_{y2} + \cos(\gamma_3+\Delta\gamma_h)\cos\Delta\gamma_v n_{z2} \end{bmatrix} \tag{29}$$

where n_{x2}, n_{y2}, and n_{z2} are three components of the unit normal vector of RA worm gear, expressed in Eq. (9).

Since $|\mathbf{n}_w^{(3)}| = 1$ and $|\mathbf{n}_w^{(2)}| = 1$, Eqs. (16)–(18) yield a system of six independent nonlinear equations with seven independent parameters, l_3, θ_3, l_1, θ_1, ϕ_1, ϕ'_3, and ϕ'_2, where l_3 and θ_3 denote the surface straight-lined edge and skew motion parameter of the mating RA worm, respectively. If the input rotation angle ϕ_3' of the RA worm is given, then other six independent parameters can be solved by numerical analysis program. In this study, the commercial software IMSL was applied to solve the aforementioned system of nonlinear equations. Finally, substituting the solved six independent parameters and ϕ_3' into Eqs. (1) and (7), the common contact point of RA worm and worm gear tooth surfaces can be obtained. At the same time, the KE of the RA worm gear drives can be calculated by applying the following equation:

$$\mathrm{KE} = \Delta\phi_2'(\phi_3') = \phi_2'(\phi_3') - \frac{\mathrm{T}_3}{\mathrm{T}_2}\phi_3' \tag{30}$$

where T_3 and T_2 are the tooth number of RA worm and worm gear, respectively. Symbol $\Delta\phi_2'(\phi_3')$ expresses the KE of RA worm gear drive, and $\phi_2'(\phi_3')$ represents the actual rotational angle of the RA worm gear under three given assembly errors, i. e., $\Delta\mathrm{C}$, $\Delta\gamma_h$, and $\Delta\gamma_h$, which can be solved by the numerical analysis program.

8.2 Investigation of CR, ICT, and ACR of RA Worm Gear Drives. The CR of an RA worm gear drive is generally defined as the average number of teeth in contact during the gear meshing. Therefore, the CR can be calculated by the rotational angle of a gear tooth, measured from the beginning contact point to the end contact point, divided by the angle formed by two successive teeth. Thus, the CR of the RA worm gear drive is defined by the following equation:

$$CR = \left(\frac{\phi_{3e}' - \phi_{3b}'}{360\ \mathrm{deg}/\mathrm{T}_3}\right) \tag{31}$$

where angles ϕ_{3e}' and ϕ_{3b}' represent the end contact point and the beginning contact point of the RA worm rotational angles, respectively. These two rotational angles can also be solved by TCA method. Therefore, $\phi_{3e}' - \phi_{3b}'$ denotes the RA worm rotational angle when RA worm gear drive is in meshing within the range of tooth surface. T_3 is the numbers of teeth of RA worm, and 360 deg/T_3 denotes the angle formed by two successive teeth of RA worm.

The TCA method can also be applied to obtain ICT and ACR of the RA worm gear drive. The ICT can be calculated at every selected computing instant (point), which is chosen as every 0.01 deg within one meshing cycle, from ϕ_{3b}' to ϕ_{3e}' of the RA worm rotational angle in this study, to check how many RA worm teeth are actually in contact with the mating RA worm gear at every instant. Thus, ICT can be considered as instantaneous contact numbers of teeth of the meshing RA worm gear drive. Herein, ACR is defined as the sum of ICT of all selected computing instants divided by the total numbers of selected computing instants within one meshing cycle of the RA worm rotational angle, from ϕ_{3b}' to ϕ_{3e}'.

8.3 Simulation of Contact Patterns. At every contact instant, the contact of mating gear tooth surfaces is spread over an elliptical area, due to their elastic deformation. Usually, the contact pattern can be investigated on a gear contact pattern testing machine. In this paper, the simulation process of bearing contacts is to determine the instantaneous contact point at first, and then the contact ellipse of the worm gear drive can be obtained by using the surface separation topology method [16]. The theoretical instantaneous contact point, solved by TCA method, is considered to be coincident with the geometrical center of bearing contact, investigated on the gear pattern testing machine.

Figure 7 schematically shows the tooth surfaces of worm Σ_3 and worm gear Σ_2 which are tangent to each other at their instantaneous contact point M_4. It is noted that the instantaneous contact point M_4 can be determined by TCA method, and the origin O_T of tangent plane coordinate system S_T can be set as the same point as instantaneous contact point M_4. Plane T denotes the common tangent plane of the two mating tooth surfaces. Symbol n_T denotes the unit normal vector of the worm and worm gear, since the unit normal vectors of the worm and worm gear tooth surfaces are collinear to each other at the perpendicular direction Z_T of tangent plane T. The calculation of contact ellipse is based on TCA results and auxiliary polar coordinate system. Let the geometrical center of a contact ellipse be the common instantaneous contact point of two mating tooth surfaces and is also considered as the origin O_T of auxiliary polar coordinate system S_T. In order to determine all the contour of contact ellipse, two other parameters r_T and θ_T of the auxiliary polar coordinates are adopted, as shown in Fig. 7(*a*). Assumed that point P is one of the boundary point of contact ellipse. Symbol r_T denotes the distance measured from the origin O_T to the boundary point of contact ellipse, and θ_T represents the angular position of boundary point of the contact ellipse. Since the coating paints on the worm tooth surface for the bearing contact test would be scraped away and printed on the worm gear tooth surface. The boundary of scraped coating paints is decided by the separation distance, measured along the Z_T axis, of two mating tooth surfaces, which is less than the size of coating paint, as shown in Fig. 7(*b*). For any angular position of θ_T, there is a point with the distance r_T at which its separation distance of two contact surfaces equals the size of coating paint for contact pattern test. In this study, the size of coating paint is chosen as 6.32 μm. For more details, the size of coating paint is considered as the sum of perpendicular distance measured from the tangent plane to the RA worm and RA worm gear tooth surfaces, individually, i.e., $d_3 + d_2$, as shown in Fig. 7(*b*). Where d_3 denotes the distance measured along the direction of Z_T axis from the searching point P of tangent plane to the point P_3 of the RA worm tooth surface Σ_3, while d_2 represents that from the same searching point P of tangent plane to point P_2 of the RA worm gear tooth surface Σ_2. Therefore, the contact ellipse can be determined by applying the following equations:

$$\mathrm{X}_T^{(3)} = \mathrm{X}_T^{(2)} = r_T \cos\theta_T \quad (-\pi \le \theta_T \le \pi) \tag{32}$$

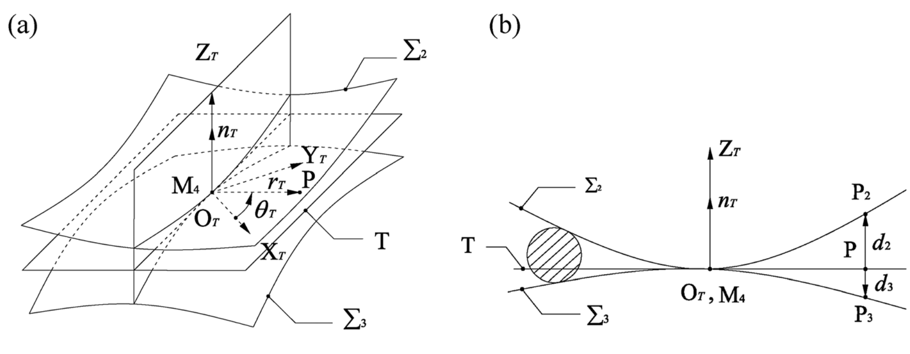

Fig. 7 (*a*) Common tangent plane and polar coordinates (*b*) measurement on surface separation distance

Table 1 Design parameters of RA worm gear drive and oversize ZN worm-type hob cutter

	RA worm	RA worm gear	Oversize hob cutter
Normal modulus	2 mm/t	2 mm/t	2 mm/t
Tooth number	1	277	1
Lead angle	3 deg	87 deg	2.86 deg
Pressure angle	10 deg	10 deg	10 deg
Tooth height	8 mm	8 mm	8 mm
Pitch radius	19.11 mm	277.38 mm	20 mm (4.7% oversize)
Cutting center distance	—		297.38 mm
Cutting crossing angle	—		89.86 deg
Meshing center distance	296.49 mm		—
Meshing crossing angle	90 deg		—

$$Y_T^{(3)} = Y_T^{(2)} = r_T \sin\theta_T \quad (-\pi \le \theta_T \le \pi) \tag{33}$$

$$|Z_T^{(2)} - Z_T^{(3)}| = 6.32\,\mu\text{m} \tag{34}$$

and

$$\tan(\theta_T) = \frac{Y_T^{(3)}}{X_T^{(3)}} \tag{35}$$

where $X_T^{(i)}$, $Y_T^{(i)}$, and $Z_T^{(i)}$ denote the position components of the RA worm ($i = 3$) and RA worm gear ($i = 2$) tooth surfaces, respectively, expressed in coordinate system S_T.

Therefore, at every instantaneous contact point M_4, the unknown parameters can be solved with Eqs. (32)–(35) by applying a numerical method. Based on the algorithm as explained above, a set of contact ellipse boundary points can be obtained, which the surface separation distance equals 6.32 μm.

9 Numerical Illustrative Examples for Worm Gear Drives Meshing Simulation

Based on the developed meshing model of the RA worm gear drive, KE, CR, ACR, ICT, and contact patterns are calculated under different assembly conditions for the following examples. Major design parameters of the RA worm gear drive and oversize ZN worm-type hob cutter are listed in Table 1.

Example 1. Semi RA, full RA, and standard proportional tooth worm gear drives, with double-depth teeth, are meshed under ideal assembly condition as follows:

Case 1: $\Delta\gamma_v = \Delta\gamma_h = 0$ deg, $\Delta C = 0$ mm (ideal assembly condition) and worm gears are generated by oversize hob cutters

The major design parameters are shown in Table 1. In this case, the worm gear drives are meshed with their respective RA worm gears that are generated by oversize ZN worm-type hob cutters, and their pitch radii are all $r_1 = 20$ mm (4.7% oversize) instead of $r_1 = 19.11$ mm.

The profile of the oversize worm-type hob cutter is based on the concept that the tooth widths of the worm and hob cutter are equal in their normal sections on the cylinder. In order to satisfy this criterion, the lead angle, cutting center distance and cutting crossing angle of the oversize worm-type hob cutter in generating the worm gear process must be modified by the following equations [9–11]:

$$\lambda_1 = \sin^{-1}\left(\frac{m_n \cos\lambda_3}{2r_1}\right) \tag{36}$$

$$C_1 = C_3 + r_1 - r_3 \tag{37}$$

and

$$\gamma_1 = \gamma_3 + \lambda_1 - \lambda_3 \tag{38}$$

where m_n denotes the normal modulus, and λ_1 and r_1 are the lead angle and pitch radius of the oversize worm-type hob cutter, and λ_3 and r_3 are of the worm, respectively. C_1 and γ_1 are cutting center distance and cutting crossing angle of the hob cutter and worm gear, respectively, while C_3 and γ_3 are meshing center distance and meshing crossing angle of the worm and worm gear, respectively. Recalled that Table 1, by substituting the given parameters m_n, r_1, r_3, λ_3, γ_3, and C_3 into Eqs. (36)–(38), one obtains parameters $\lambda_1 = 2.86$ deg, $C_1 = 297.38$ mm, and $\gamma_1 = 89.86$ deg of the oversize ZN worm-type hob cutter. The rest of design parameters of RA worm gear drive and oversize ZN worm-type hob cutter are also shown in Table 1.

It is noted that the semi RA, full RA, and standard proportional tooth worm gear drives of case 1 are meshed under ideal assembly condition, but their meshing is all in point contacts, since their mating RA worm gears are generated by an oversize ZN worm-type hob cutter herein. Therefore, the KEs of mating gear drives are nonzero according to the TCA results. The solved meshing parameters, KEs and CRs are all summarized in Table 2. KEs of these three types of worm gear drives are shown under some specified worm rotational angles, ϕ_3'. By applying Eq. (31), it is found that the full RA worm gear drive has maximum CR = 7.58 (since its corresponding worm rotational angles are $\phi_{3b}' = 15.64$ deg and $\phi_{3e}' = 2745.81$ deg) in case 1, while the semi RA and standard proportional tooth worm gear drives have CR = 7.39 (correspondingly, $\phi_{3b}' = -569.03$ deg and $\phi_{3e}' = 2089.77$ deg) and CR = 6.91 (correspondingly, $\phi_{3b}' = -1053.29$ deg and $\phi_{3e}' = 1433.26$ deg), respectively. Three terms "STD," "SEMI," and "FULL," appeared

Table 2 Kinematic errors and bearing contacts of three types of worm gear drives for case 1

	ϕ_3' (deg)	l_3 (mm)	θ_3 (deg)	ϕ_3' (deg)	l_1 (mm)	θ_1 (deg)	KE (arc-sec)	CR
Std	−800.0	6.3120	−797.4533	−2.8880	6.3148	−803.5230	0.3102	6.91
	−400.0	7.5492	−398.8153	−1.4440	7.5498	−401.4447	0.0701	
	0	8.7733	0	0	8.7732	−0.0002	0	
	400.0	9.9884	398.9577	1.4441	9.9888	401.0173	0.0589	
	800.0	11.1973	798.0322	2.8881	11.1988	801.7385	0.2181	
Semi	0	6.8036	0	0	6.8036	−0.0001	0	7.39
	400.0	8.0187	398.9608	1.4441	8.0191	401.0128	0.0587	
	800.0	9.2277	798.0377	2.8882	9.2291	801.7315	0.2173	
	1200.0	10.4324	1197.2115	4.3324	10.4353	1202.2409	0.4552	
	1600.0	11.6341	1596.4673	5.7766	11.6387	1602.5987	0.7569	
Full	400.0	6.0490	398.9639	1.4441	6.0494	400.0083	0.0585	7.58
	800.0	7.2580	798.0433	2.8882	7.2595	801.7246	0.2165	
	1200.0	8.4628	1197.2190	4.3323	8.4657	1202.2329	0.4537	
	1600.0	9.6646	1596.4762	5.7764	9.6691	1602.5904	0.7545	
	2000.0	10.8644	1995.8032	7.2205	10.8706	2002.8372	1.1073	

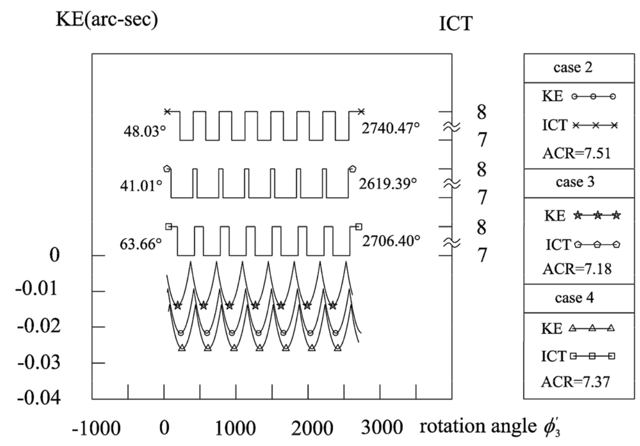

Fig. 8 Kinematic errors of full RA worm gear drives

in Table 2, denote the meshing of standard proportional tooth, semi RA and full RA worm gear drives, respectively.

Example 2. A full RA worm gear drive with double-depth teeth, which the RA worm gear is generated by an oversize ZN worm-type hob cutter, and its pitch radius is $r_1 = 20$ mm (4.7% oversize), is meshed under the following three error assembly conditions:

Case 2: $\Delta\gamma_v = \Delta\gamma_h = 0$ deg, $\Delta C = -0.1$ mm

Case 3: $\Delta\gamma_v = -3'$, $\Delta\gamma_h = 3'$, $\Delta C = -0.1$ mm

Case 4: $\Delta\gamma_v = 3'$, $\Delta\gamma_h = -3'$, $\Delta C = -0.1$ mm

In this example, the major design parameters are all chosen the same as those of Table 1. The simulated TCA results and bearing contacts are shown in Figs. 8 and 9, respectively. Figure 8 shows the KEs, ICTs, and ACRs of a full RA worm gear drive under three assembly conditions of cases 2–4, respectively. It is found that the contact begins at 48.03, 41.01, and 63.66 deg, and ends at 2740.47, 2619.39, and 2706.40 deg, of the full RA worm rotational angles, ϕ_3', respectively, for cases 2–4. Therefore, their corresponding CRs, calculated by Eq. (31), are 7.48, 7.16, and 7.34, respectively. The maximum KEs of cases 2–4 are 0.0124, 0.0123, and 0.0123 arc-sec, respectively. ICTs are all varied between 7 and 8 teeth for cases 2–4, and ACRs are 7.51, 7.18, and 7.37, respectively, as shown in Fig. 8. It is found that ACRs are slightly larger than CRs for the full RA worm gear drive under three error assembly conditions of cases 2–4.

Figure 9 illustrates the contact loci and their corresponding contact ellipses on the full RA worm gear surface for cases 2–4. In order to clearly show the contact loci and contact ellipses, the full RA worm rotational angles ϕ_3' are partially chosen from 600 deg to 1400 deg, with an interval of 200 deg for cases 2–4. For case 2, its contact locus and contact ellipses are located near the middle

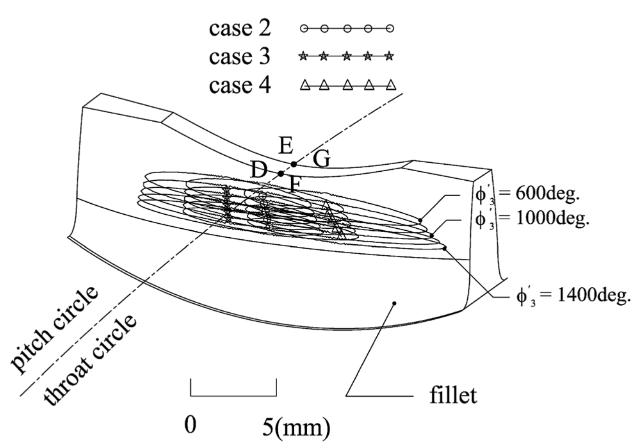

Fig. 9 Contact patterns and loci of full RA worm gear drives

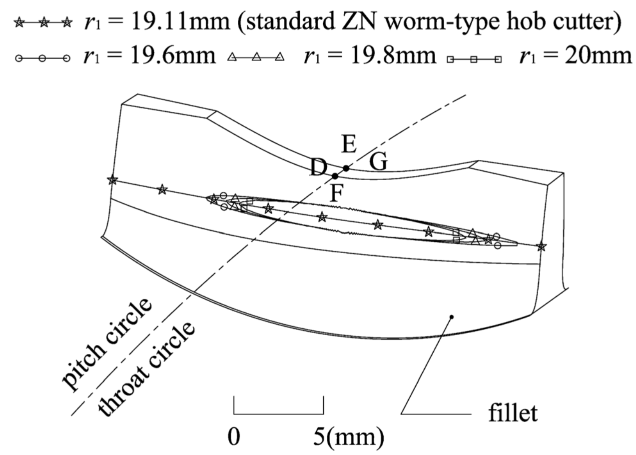

Fig. 10 Contact ellipses on tooth flank of the full RA worm gear generated by different pitch radii of oversize ZN worm-type hob cutters

section of the full RA worm gear face width, while those of cases 3 and 4 are shifted to the left and right sides of the full RA worm gear face width, respectively.

Example 3. Comparison of contact ellipse sizes of the full RA worm gear drive with double-depth teeth that is meshed under ideal assembly condition, as shown in case 5. Case 5: $\Delta\gamma_v = \Delta\gamma_h = 0$ deg, $\Delta C = 0$ mm (ideal assembly condition)

It is noted that the full RA worm gears are generated by different pitch radii, $r_x = 19.11$ mm (standard ZN worm-type hob cutter), 19.6 mm, 19.8 mm, and 20 mm, respectively, of oversize ZN worm-type hob cutters.

Corresponding design parameters of the hob cutter are calculated by Eqs. (36)–(38), and some major design parameters of the worm gear drive are listed in Table 1. As displayed in Fig. 10, the contact ellipses are shown at the RA worm rotational angle $\phi_3' = 1000$ deg under ideal assembly condition of case 5. A full RA worm gear drive is in line contact, since its worm gear is generated by a standard ZN worm-type hob cutter ($r_1 = 19.11$ mm). However, if the mating worm gears are generated by oversize hob cutters ($r_1 = 19.6$ mm, 19.8 mm, and 20 mm), the contacts of the full RA worm gear drive tend to contact ellipses. The contact ellipses become smaller, i.e., smaller contact area, when the pitch radius of the oversize ZN worm-type hob cutter increases. It is found that variation of r_1 has not too much effect on the length of minor axis of contact ellipses. In the other words, the contact area mainly depends on the length of major axis of contact ellipses. It is noted that the contact stress can be decreased by increasing of a large contact area on the contact tooth surface of full RA worm gear by choosing a suitable pitch radius of the oversize ZN worm-type hob cutter. The contact area of contact ellipse and ICT is two key factors in the gear tooth contact stress prediction. When the pitch radius r_1 of the oversize ZN worm-type hob cutter tends to $r_1 = r_3 = 19.11$ mm (i.e., a standard RA worm), the line contact occurs, and edge contact may happen under gear drive assembly errors.

10 Conclusion

The worm gear of an RA worm gear drive is generally generated by a standard ZN worm-type hob cutter. It results in line contact and easily induces edge contact of the gear drive meshing. In order to overcome this defect, the worm gear pair is proposed herein by adopting the RA worm meshing with the RA worm gear, which is generated by an oversize ZN worm-type hob cutter. Then, the worm gear drive becomes in point contact under ideal even error assembly conditions.

In this study, the KE, CR, ACR, ICT, and contact patterns of the RA worm gear drive with double-depth teeth, are investigated by applying the developed TCA computer programs. It is found that the CR, ACR, and ICT of the RA worm gear drive are significantly higher than those of the conventional worm gear drive because of multiteeth of contact, and KEs are dramatically lower under various gear assembly errors. It is worth mentioning that ACRs are slightly larger than CRs, which are calculated by conventional definition.

Effects of worm gear drive assembly errors and major RA worm gear design parameters on the dimensions of contact ellipses are investigated by applying the developed TCA computer simulation programs and surface separation topology method. Besides, the major-axis length of contact ellipse can be adjusted by changing the pitch radius of an oversize ZN worm-type hob cutter, but the minor-axis length of contact ellipse has not too much affected by the pitch radius variation of an oversize ZN worm-type hob cutter. Thus, by properly choosing the pitch radius for the oversize ZN worm-type hob cutter to generate the worm gear, the area of the contact ellipse can be increased significantly, and it can avoid the edge contact even under severely gear drive assembly errors.

References

[1] Buckingham, E. K., 1971, "Here's How to Design Full and Semi-Recess Action Gears," *Gear Design and Application*, N. P. Chironis, ed., Product Engineering Magazine, McGraw-Hill, New York, pp. 136–143.

[2] Buckingham, E. K., 1971, "3 Are Familiar, 3 Little Known in This Guide to Worm Gear Types," *Gear Design and Application*, N. P. Chironis, ed., Product Engineering Magazine, McGraw-Hill, New York, pp. 69–78.

[3] Crosher, W. P., 2002, *Design and Application of the Worm Gear*, ASME, New York, pp. 123–126.

[4] Litvin, F. L., *Theory of Gearing NASA Reference Publication 1212*, (U.S. Government Printing Office, Washington, DC, 1989).

[5] Litvin, F. L., and Fuentes, A., 2004, *Gear Geometry and Applied Theory*, 2nd ed., Cambridge University Press, Cambridge, UK.

[6] Litvin, F. L., and Kin, V., 1990, *Computerized Simulation of Meshing and Bearing Contact for Single-Enveloping Worm Gear Drives*, ASME, Design Engineering Division, DE, Vol. 26, pp. 423–432.

[7] Tsay, C. B., 1988, "Helical Gear With Involute Shaped Teeth: Geometry, Computer Simulation, Tooth Contact Analysis and Stress Analysis," ASME J. Mech., Transm., Autom. Des., **110**(4), pp. 482–491.

[8] Lin, C. Y., Tsay, C. B., and Fong, Z. H., 1996, "Tooth Contact Analysis of Hypoid Gears," J. Chin. Soc. Mech. Eng., **110**(3), pp. 241–249.

[9] Fang, H. S., and Tsay, C. B., 2000, "Mathematical Model and Bearing Contacts of the ZN-Type Worm Gear Set Cut by Oversize Hob Cutters," Mech. Mach. Theory, **35**(12), pp. 1689–1708.

[10] Fang, H. S., and Tsay, C. B., 1996, "Effects of the Hob Cutter Regrinding and Setting on ZE-Type Worm Gear Manufacture," Int. J. Mach. Tools Manuf., **36**(10), pp. 1123–1135.

[11] Fang, H. S., and Tsay, C. B., 1996, "Mathematical Model and Bearing Contacts of the ZK-Type Worm Gear Set Cut by Oversize Hob Cutters," Mech. Mach. Theory, **31**(3), pp. 271–282.

[12] Fang, H. S., and Tsay, C. B., 1995, "Bearing Contact and Kinematic Error of ZE-Type and ZK-Type Combination Worm Gear Sets," J. Chin. Soc. Mech. Eng. Trans. Chin. Inst. Eng. Ser. C, **16**(4), pp. 327–335.

[13] Shigley, J. E., and Mischke, C. R., 1989, *Mechanical Engineering Design*, 5th ed., McGraw-Hill, NY.

[14] Bair, B. W., and Tsay, C. B., 1998, "ZK-Type Dual-Lead Worm and Worm Gear Drives: Contact Teeth, Contact Ratios and Kinematic Errors," ASME J. Mech. Des., **120**(3), pp. 422–428.

[15] Bair, B. W., and Tsay, C. B., 2001, "Effects of Profile Shifted Factor and Pressure Angle on the ZK-Type Dual-Lead Worm Gear Drives," J. Mater. Process. Technol., **112**(1), pp. 29–36.

[16] Janninck, W. L., 1988, "Contact Surface Topology of Worm Gear Tooth," Gear Technol., **5**(2), pp. 31–47.

[17] Litvin, F. L., Seol, I. H., Kim, D., Lu, J., Wang, G A., Egelja, A., Zhao, X., and Handschuh, R. F., 1996, "Kinematic and Geometric Models of Gear Drives," ASME J. Mech. Des., **118**, pp. 544–550.

[18] Chen, K. Y., and Tsay, C. B., 2009, "Contact Characteristics of the ZK-Type Worm and ZN-type Worm Wheel Meshing With a Non-Ninety-Degree Crossing Angle," *Proceedings of MPT2009-Sendai, JSME International Conference on Motion and Power Transmissions*, pp. 534–539.

[19] Colbourne, J. R., 1989, "The Use of Oversize Hobs to Cut Worm Gears," American Gear Manufactures Association Conference, Virgina.

[20] Simon, V., 1996, *Characteristics of a New Type of Cylindrical Worm Gear Drive*, ASME, Design Engineering Division, DE, Vol. 88, pp. 133–140.

[21] Litvin, F. L., Yukishima, K., Hayasaka, K., Gonzalez-Perez, I., and Fuentes, A., 2007, "Geometry and Investigation of Klingelnberg-Type Worm Gear Drive," ASME J. Mech. Des., **129**(1), pp. 17–22.

[22] Seol, I. H., and Litvin, F. L., 1996, *Computerized Design, Generation and Simulation of Meshing and Contact of Modified Involute, Klingelnberg and Flender Type Worm-Gear Drives*, ASME, Design Engineering Division, DE, Vol. 88, pp. 125–131.

[23] Seol, I. H., 2000, "Design, Generation and Simulation of Meshing of Worm-Gear Drive With Longitudinally Localized Contacts," ASME J. Mech. Des., **122**(2), pp. 201–206.

[24] Yang, Y., 1995, "Computer-Aided Design of Recess-Action Gears," *Computers in Engineering, Proceedings of the International Computers in Engineering Conference*, Vol. 3, pp. 445–449.

[25] Siegal, R. E., and Mabie, H. H., 1973, "Determination of Hob-Offset Values for Nonstandard Spur Gears Based on Maximum Ratio of Recess to Approach Action," Appl Mech Conf, 3rd, Proc, Pap, Stillwater.

[26] Meng, H., and Chen, Q., 1984, "Research into the Scuffing Loading Capacity of All-Recess Action Gears," *Proceedings of the Sixth World Congress on the Theory of Machines and Mechanisms*, New Delhi, India, pp. 895–901.